Biochimica et Biophysica Acta 1848 (2015) 1451–1461

Contents lists available at ScienceDirect

Biochimica et Biophysica Acta

journal homepage: www.elsevier.com/locate/bbamem

Structure–function relationships in histidine-rich antimicrobial peptides from Atlantic cod

Mark McDonald [a], Michael Mannion [a], Damien Pike [a], Krystina Lewis [a], Andrew Flynn [a], Alex M. Brannan [a], Mitchell J. Browne [a], Donna Jackman [a], Laurence Madera [c], Melanie R. Power Coombs [b], David W. Hoskin [b,c,d], Matthew L. Rise [e], Valerie Booth [f,*]

[a] Department of Biochemistry, Memorial University of Newfoundland, St. John's, NL A1B 3X9, Canada
[b] Department of Pathology, Dalhousie University, Canada
[c] Department of Microbiology and Immunology, Dalhousie University, Canada
[d] Department of Surgery, Dalhousie University, Canada
[e] Ocean Sciences Centre, Memorial University of Newfoundland, St. John's, NL A1B 3X9, Canada
[f] Department of Physics and Physical Oceanography, Memorial University of Newfoundland, St. John's, NL A1B 3X9, Canada

ARTICLE INFO

Article history:
Received 14 November 2014
Received in revised form 10 March 2015
Accepted 22 March 2015
Available online 1 April 2015

Keywords:
Antimicrobial peptide
Minimal inhibitory concentration (MIC) assay
Cancer cell killing
Peptide structure
Solution NMR
Circular dichroism

ABSTRACT

Gad-1 and Gad-2 are antimicrobial peptide (AMP) sequences encoded by paralogous genes. They are rich in histidine, which suggests that their activity might be pH-dependent. We examined their structure–function relationships with a view to learning how to improve AMP therapeutic ratios. Activity assays with Gram-negative bacteria and cancer cell lines demonstrate that Gad-2 is substantially more active at slightly acidic pH than it is at neutral pH. By contrast, the activity of Gad-1 at lower pH is similar to its activity at pH 7. Circular dichroism spectra indicate that the greater functional plasticity of Gad-2 correlates with a greater structural plasticity; Gad-2's percent helicity varies dramatically with altered pH and lipid environment. Interestingly, Gad-2's highest levels of helicity do not correspond to the conditions where it is most active. High resolution solution NMR structures were determined in SDS micelles at pH 5, conditions that induce an intermediate level of helicity in the peptides. Gad-1 is more helical than Gad-2, with both peptides exhibiting the greatest helical tendencies in their central region and lowest helicity in their N-termini. The high resolution structures suggest that maximum activity relies on the appropriate balance between an N-terminal region with mixed hydrophobic/hydrophilic structure features and an amphipathic central and C-terminal region. Taken together with previous studies, our results suggest that to improve the therapeutic ratio of AMPs, consideration should be given to including sequential histidine-pairs, keeping the overall charge of the peptide modest, and retaining a degree of structural plasticity and imperfect amphipathicity.

1. Introduction

Antimicrobial peptides (AMPs) are a component of many organisms' innate immune systems. They are one of the most ancient defense mechanisms we have against pathogenic organisms such as bacteria, viruses and fungi, and some have also been observed to have anti-cancer properties [1–3]. Because of their efficacy they have survived the evolutionary process even in organisms with highly complex immune systems. Many AMPs display specificity for pathogenic cells over host cells, in large part due to differences in cell membrane composition. AMP-membrane interactions are key in AMP mechanisms, either via direct AMP killing by membrane disruption, or in order to gain entry to the target cell to access intracellular targets [4]. Considering the widespread decrease in the efficacy of conventional antibiotics [5], this membrane-specific property of AMPs makes them a highly attractive alternative and therefore of great interest in the area of therapeutic drugs. There has been success in developing and licensing AMP therapeutics for topical use [6], but, thus far, the development of injectable AMP therapeutics has been hampered by the level of toxicity associated with AMPs [7]. In other words, although many AMPs are more specific for their target microbes than for the host cells, their therapeutic ratios are still insufficiently high. Our studies of the AMPs Gad-1 and Gad-2 are thus designed with a view to better understanding the mechanisms for their specificity and thus supporting the development of higher therapeutic ratio AMPs.

Gad-1 and Gad-2 are AMP sequences encoded by paralogous genes previously identified from an Atlantic cod (*Gadus morhua*) expressed sequence tag database [8]. Their importance to Atlantic cod innate immunity is supported by their high constitutive transcript expression in spleen, head kidney, gill, and blood and their up-regulation after stimulation with bacterial antigens [8]. One interesting feature of the

* Corresponding author.
E-mail address: vbooth@mun.ca (V. Booth).

http://dx.doi.org/10.1016/j.bbamem.2015.03.030
0005-2736/

Gad peptides is that they each possess several histidine residues — Gad-1 has five and Gad-2 has four. Histidine is noted for having a pH-dependent charge and therefore the electrostatic interaction with a charged membrane surface could depend on pH. Such histidine-rich peptides are of interest in terms of understanding the physiological control of AMP activity [9], in their potential for treating solid tumors, which usually have an acidic environment [10,11], as well as in their power to reveal the role of charge interactions in model studies by allowing us to tune the charge of the AMP. Previously identified natural histidine-rich AMPs include the human salivary peptide family of histatins [12,13]; the root peptides shepherin I and shepherin II [14]; histidine-rich glycoprotein [15]; AMPs from ticks [16,17]; and clavanins [18,19]. Other studies have focused on introducing non-native histidines into peptides in place of Arg or Lys residues of native sequences or incorporating histidines into designed sequences [20–23]. Such studies have suggested at least three different mechanisms for altered histidine-rich-AMP activity with pH: 1) alterations in membrane binding; 2) alterations in membrane penetration; and 3) alterations in peptide structure.

In addition to alterations in activity with pH, also of interest are the differences in activity between Gad-1 and Gad-2. Since they are encoded by paralogous genes, we might expect their specificities to be tuned to different pathogens. This possibility was investigated in antimicrobial assays of four Gram-positive and eight Gram-negative bacterial strains plus a protozoan, that employed peptides that were only slightly different from those used in the current study; Gad-1 in the earlier study had an additional C-terminal Gly and Gad-2 in the earlier study lacked the C-terminal Arg [24]. The authors found that while the Gad-1-like peptide was broadly active against bacteria, the Gad-2-like peptide was not; the latter peptide exhibited higher activity against the parasite [24]. The Gad peptides belong to a large family of related, but diverse AMPs from fish, termed piscidins [25]. The most studied, in terms of structural mechanisms, is a piscidin with 41% identity to Gad-1 and 27% identity to Gad-2 [26]. It forms an amphipathic helix that disrupts anionic bilayers [27], but to our knowledge alterations in this behavior with pH have not been examined. Notably, this piscidin's activity seems to depend on retaining conformational flexibility [28]. Several studies point to conformational flexibility as an important factor in AMP specificity [29–31] and thus in our studies of Gad peptide structure–function mechanisms we need to keep in mind that the most well-structured conformations of AMPs are not necessarily the most biologically relevant conformations. While much work has been carried out exploring the mechanisms of membrane disruption by AMPs, including toroidal pore, carpet, and lipid clustering [32,33], at this date, the particular mechanism(s) employed by Gad-1 and Gad-2 are unknown.

A major reason for the paucity of clinical success with injected AMP-based therapeutics is the level of toxicity associated with AMPs [7]. Although many AMPs are more specific for their target microbes than for the host cells, their therapeutic ratios are still insufficiently high. The peptides Gad-1 and Gad-2 have potential to teach us about how specificity is tuned in natural peptides and thus may provide us with lessons we can apply to improve the therapeutic ratio of other peptides in development for use in humans. The first consideration for specificity-tuning in Gads is their histidine residues, which introduce the possibility to alter charge interactions, and hence activity, by changing the pH. Secondly, Gad-1 and Gad-2 are paralogous genes, and although they retain some sequence similarity, they have also apparently evolved different specificities in target microbes [24]. In order to better understand specificity-tuning in the Gad peptides, we have assayed the pH dependence of their anti-bacterial and anti-cancer activities, used circular dichroism to learn how their helicity is altered with changes in pH or lipid environment, and applied solution NMR to determine the high resolution structures of the peptides in conditions that lead to an intermediate level of helicity.

2. Experimental methods

2.1. Peptide preparation

Putative mature Gad-1 (FIHHIIGWISHGVRAIHRAIH-NH_2), and Gad-2 (FLHHIVGLIHHGLSLFGDR-NH_2) were produced by solid-phase synthesis using O-fluorenylmethyloxycarbonyl (Fmoc) chemistry. For each peptide, Fmoc amino acids were weighed out in 5× excess and placed into a CS Bio peptide synthesizer (model CS336X, CS Bio Company Inc., Menlo Park, CA) using 0.43 g of a 0.47 mmol/g rink amide resin (CS Bio Company Inc., Menlo Park, CA). Dissolution of amino acids was facilitated with 0.4 M 1-hydroxy-benzotriazole (HoBt) dissolved in dimethylformamide (DMF). De-blocking of amino acids was performed with 20% piperidine/DMF (Sigma-Aldrich Co., St. Louis MO). Resin washes were carried out with DMF. Upon completion of peptide synthesis, the resin containing peptide was transferred to a 10 mL syringe (BD Diagnostics Co.) equipped with a filter, and washed with methanol thoroughly under vacuum. The resin was then air dried for 30 min followed by vacuum desiccation for 60 min. Cleavage of the peptide from the resin was carried out using a solution of 9.4 mL trifluoroacetic acid (TFA), 0.25 mL 1,2-ethanedithiol, 0.1 mL thioanisole (Sigma-Aldrich Co.), and 0.25 mL distilled water. The cleavage solution (5.0 mL) was added to the resin and stirred for 2 h. The resulting solution, which contained the C-terminally amidated peptide, was then extruded through the syringe into a 50 mL Falcon tube (Fisher, Toronto ON). The peptide was then precipitated with the addition of 40 mL of −20 °C diethyl ether, and the tube was incubated at −20 °C overnight. The precipitate was then pelleted by centrifugation at 4 °C at 2000 *g* for 5 min, the supernatant removed, and two further ether precipitations were performed, each for 4 h. The resulting pellet was air-dried overnight, re-suspended in double distilled water with 0.1% TFA (Sigma-Aldrich Co.), and filtered using a glass fiber Acrodisc syringe filter (Pall Canada Ltd., Ville St. Laurent, QC).

Peptide purification was performed using high-pressure liquid chromatography (HPLC) (Varian ProStar HPLC, Varian Inc., St. Laurent, QC) equipped with a reverse-phase DYNAMAX C-8 preparatory column (Varian Inc., St. Laurent, QC). Peptides were eluted at a wavelength of 215 nm using an acetonitrile gradient (80/20% HPLC grade water/acetonitrile — 0/100% acetonitrile; Sigma-Aldrich Co) with monitoring at a wavelength of 215 nm and desalted by dialysis against 5% acetic acid and then water. The mass of each peptide was confirmed via matrix assisted laser desorption ionization — time of flight mass spectrometry (MALDI-TOF MS — Genomics and Proteomics facility, Memorial University). Final purity of the peptides was determined to be >95% by analytical HPLC.

2.2. MIC assays

Minimal inhibitory Concentration (MIC) assays were carried out using JM109 *Escherichia coli*. The working concentration of bacteria was 5×10^5 cfu/mL in Mueller Hinton (MH) broth. Two-fold serial dilutions of peptides Gad-1 and Gad-2 were carried out in untreated sterile 96-well polypropylene plates where 10 μL of peptide was plated with 90 μL of bacteria. The concentrations varied from 50 to 0.1 μg/mL (20.24 μM to 2.53 μM for Gad-1 and 23.04 μM to 2.88 μM for Gad-2). Controls included buffer only and MH broth only. The plates were incubated at 37 °C in a shaking incubator set at 140 RPM for 16 h. The MIC was defined as the lowest concentration of peptide that resulted in no bacterial culture growth as judged by visual inspection of the opacity. Each plate had duplicate rows and the plates were run in triplicate. Assays were completed at pH 5 and pH 7.

2.3. Hemolytic assay

Fresh human red blood cells (RBCs) were washed three times in 150 mM NaCl + 20 mM Tris–HCl (Sigma-Aldrich Co) and resuspended

in 100 mM sodium phosphate buffer at pH 7 (PB) at a concentration of 5×10^8 RBC/mL. Two hundred microliters of RBC suspension was added to 1.3 mL of peptide to give the appropriate final concentration of peptide as quoted in Table 1. The positive control (100% lysis) was 200 μL of RBC suspension plus 1.3 mL of 1% Triton X-100 (Sigma-Aldrich) and the negative control (0% lysis) was 200 μL of RBC suspension plus 1.3 mL of PB. The solutions were placed in a 37 °C water bath for an hour and centrifuged at 850 g for 10 min at 4 °C. The supernatants were collected by pipette, transferred to cuvettes and absorbance measured at 541 nm using a Genesys 10S UV–VIS Thermo Scientific Spectrometer. Percent hemolysis was calculated as:

$$\left(\frac{\text{Absorbance of sample–Absorbance of negative control}}{\text{Absorbance of positive control}}\right) \times 100\%$$

2.4. Cell culture and conditions

Murine Lewis lung carcinoma cells (LLC) and human prostate PC3 cancer cells were obtained from ATCC (Manassas, VA, USA). Human ovarian HEY cancer cells were a kind gift from Dr. M. Nachtigal (University of Manitoba,Winnipeg, MB, Canada). LLC, PC3 and HEY cells were maintained in a 37 °C incubator with a 10% CO_2 humidified atmosphere in DMEM culture medium (Sigma-Aldrich, Oakville, ON, Canada) supplemented with 10% heat-inactivated fetal bovine serum (FBS), 100 U/mL penicillin, 100 μg/mL streptomycin, 2 mM L-glutamine, and 5 mM 4-(2-hydroxyethyl)-1-piperazineethanesulfonic acid (HEPES) at pH 7.4 (all from Invitrogen, Burlington, ON, Canada), referred to as cDMEM. LLC, PC3 and HEY were cultured in T75 tissue culture flasks (Sarstedt, QC, Canada) and were passaged as required, with cell confluence never exceeding 90%. U266 multiple myeloma cells were kindly provided by Dr. Tony Reiman (Saint John Regional Hospital, Saint John, NB, Canada). U266 cells were maintained at 37 °C in a 5% CO_2 humidified atmosphere in RPMI 1640 medium (Sigma-Aldrich Canada, Oakville, ON, Canada) supplemented with 5% heat-inactivated FBS, 5 mM HEPES (pH 7.4), 100 U/mL penicillin and 100 μg/mL streptomycin (Invitrogen, Burlington, ON, Canada), referred to as cRPMI. Stock flasks were passaged as required to maintain optimal cell growth. All cells were routinely shown to be free of mycoplasma contamination.

2.5. MTT viability assay

LLC, HEY, and PC3 cancer cells were seeded into 96-well flat-bottom plates (Thermo Scientific, Rochester, NY, USA) at 2×10^4 cells per well and incubated overnight. Culture supernatants were then removed and replaced with cDMEM adjusted to pH 6 or 7. Cells were then cultured in the absence or presence of the indicated concentrations of Gad-1 or Gad-2 for 24 h. At the end of culture, supernatants were removed and replaced with fresh cDMEM, and thiazol blue tetrazolium bromide (MTT; Sigma Aldrich, ON, Canada) was added to each well (0.5 mg/mL). The cells were incubated for 2 h to allow for the formation of formazan crystals by mitochondrial dehydrogenases. Cells were centrifuged for 5 min at 500 ×g and the supernatants removed. Formazan crystals were then solubilized with the addition of 100 μL of DMSO to each well. The absorbance at 570 nm, as an indicator of live cells, was measured using an ASYS Expert 96-well plate reader (Montreal Biotech Inc., Dorval, QC, Canada). Cytotoxicity was calculated with the following equation $[1\text{-}(A570_{\text{treatment}} / A570_{\text{vehicle}})]100$, for each pH condition. Each treatment condition was done in triplicate.

Table 1
Percent helicity of AMPs estimated from the ellipticity at 222 nm [35].

	pH	Gad-1	Gad-2
Buffer	5	7%	4%
20% TFE	5	16%	12%
20 mM SDS	5	25%	12%
POPC	5	37%	7%
POPC	6	35%	10%
POPC	7	42%	16%
POPG	5	56%	19%
POPG	6	79%	36%
POPG	7	100%	100%

2.6. 7-AAD death assay

U266 cells were incubated in 24-well plates (5×10^5 cells per well) for 1 h with vehicle, 50 μM Gad-1 or Gad-2 at 37 °C in a 5% CO_2 humidified atmosphere in RPMI-1640 + 0.5% FBS at pH 6 or 7. Cells were stained with 7-AAD (eBioscience) 5 min before analysis by FACSCalibur flow cytometer (BD Biosciences, Mississauga, ON). The percentage of dead cells were gated based on the live vehicle control cells.

2.7. Circular dichroism

The secondary structures of Gad-1 and Gad-2 were assessed in a variety of environments using far-ultraviolet circular dichroism (CD) spectroscopy [34]. To prepare the samples with lipids, lyophilized 1-palmitoyl-2-oleoyl-*sn*-glycero-3-phosphocholine (POPC) or 1-palmitoyl-2-oleoyl-*sn*-glycero-3-phospho-(1′-rac-glycerol) (POPG) (Avanti Polar Lipids Inc., Alabaster, Al) was dissolved in 20 mM pH 5 dibasic phosphate buffer to a concentration of 25 mM, and subjected to five freeze-thaw cycles. The resulting liposome solutions were extruded through a 200 nm filter (Nuclepore Track-Etched Membranes, Whatman, Toronto ON) under nitrogen gas pressure to make large unilamellar vesicles (LUVs). Appropriate volumes of the LUV solutions were mixed with peptide stock solution to give a final lipid concentration of 1.4 mM and a final peptide concentration of 30 μM and the pH adjusted as necessary. CD experiments were also performed with 30 μM peptide in buffer alone, with 20 mM sodium dodecyl sulfate (SDS) micelles, and with 20% trifluoroethanol (TFE). Spectra were collected (20 per analysis) in millidegrees using a Jasco J-810 spectropolarimeter (Jasco Inc., Easton, MD) in the far ultraviolet range (190–260 nm) with a 0.5 mm quartz cuvette at 25 °C. All sample preparations and CD spectra acquisitions were repeated at least once — the spectra shown in Fig. 5 are representative scans.

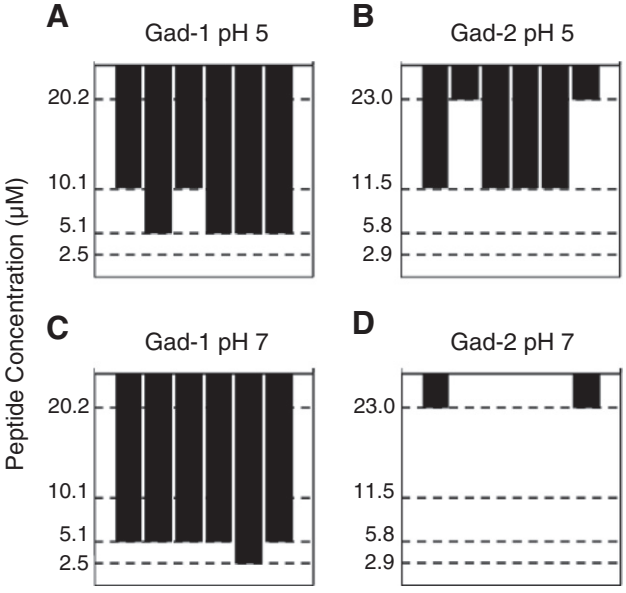

Fig. 1. Minimal inhibitory concentration (MIC) for peptides to prevent growth of *E. coli* for (A) Gad-1 at pH 5, (B) Gad-2 at pH 5, (C) Gad-1 at pH 7 and (D) Gad-2 at pH 7. Each bar represents one of six replicate experiments and the length of the bars indicates the minimum peptide concentration required to inhibit bacterial growth. No bar indicates an MIC greater than 50 μg/mL (20.2 μM for Gad-1 and 23.0 μM for Gad-2).

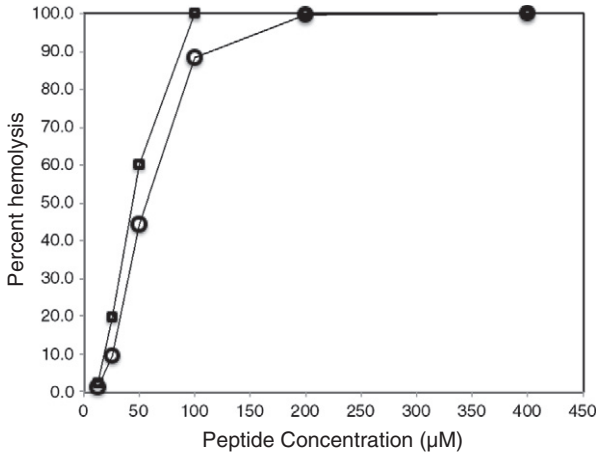

Fig. 2. Hemolytic activity of Gad-1 (square symbols) and Gad-2 (circles) after 1 h incubation time at 37 °C.

Spectra were normalized by subtracting a baseline and then converting the units to mean-residue ellipticity (MRE) according to $MRE = \theta/(c \times l \times N_r)$, where θ is the recorded ellipticity, c is the peptide concentration in dmol/L, l is the cell path-length in cm, and N_r is the number of residues in the peptide. Percent helicity was estimated from the normalized CD spectra based on the empirical formulae given in [35], i.e. $f_H = (\theta_{222} - \theta_C)/(\theta_H - \theta_C)$, with $\theta_C = 2200 - 53\ T$ and $\theta_H = (-44{,}000 + 250\ T)(1 - 3/N_r)$ where T is the temperature in °C, f_H is the fraction of helical structure, and θ_{222} is the MRE at 222 nm.

2.8. NMR experiments

Peptides (2 mM) were dissolved in buffers of 90/10% H_2O/D_2O (for NOESY experiments) or 100% D_2O (for TOCSY experiments) plus 150 mM deuterated sodium dodecyl sulfate (SDS) (Cambridge Isotope Laboratories, Andover, MA) and 0.2 mM 4,4-dimethyl-4-silapentane-1-sulfonic acid (DSS) as an internal reference, and adjusted to pH 5. Samples were loaded into 5 mm thin-walled glass NMR tubes (Norell Inc. Landisville, NJ). One-dimensional (1D) ^1H and two-dimensional (2D) NOESY and TOCSY spectra of the peptides in SDS micelles were obtained using a Bruker Avance 600 MHz spectrometer equipped with a TXI probe. For 1D ^1H NMR, 16 scans were used. For 2D TOCSY experiments, a DIPSI2 spin-lock sequence was used, with a mixing time of 80 ms, and 128 scans accumulated. For the 2D NOESY experiments, a mixing time of 150 ms was used with 472 scans. All 2D experiments had a recycle delay of 1 s. Spectra were processed using iNMR (http://www.inmr.net) and analyzed with SPARKY [36].

2.9. Structure determination

Chemical shift assignments were assigned via standard methods [37] using 2D TOCSY and NOESY data acquired in 90% H_2O and 10% D_2O as well as 100% D_2O at 35 °C, with help from the same experiments at 40 °C and 45 °C in order to resolve ambiguities. NOEs were quantified using peak height from the 90/10% H_2O/D_2O NOESY spectra at 35 °C. The NOEs were divided into three classes corresponding to strong, medium and weak intensities and assigned target distances of 1.8–2.5 Å, 1.8–3.5 Å and 1.8–5.0 Å respectively. In order to avoid overconstraining the peptide structures, the calculations were carried out with some alterations to the "standard" NMR structure calculation methods for

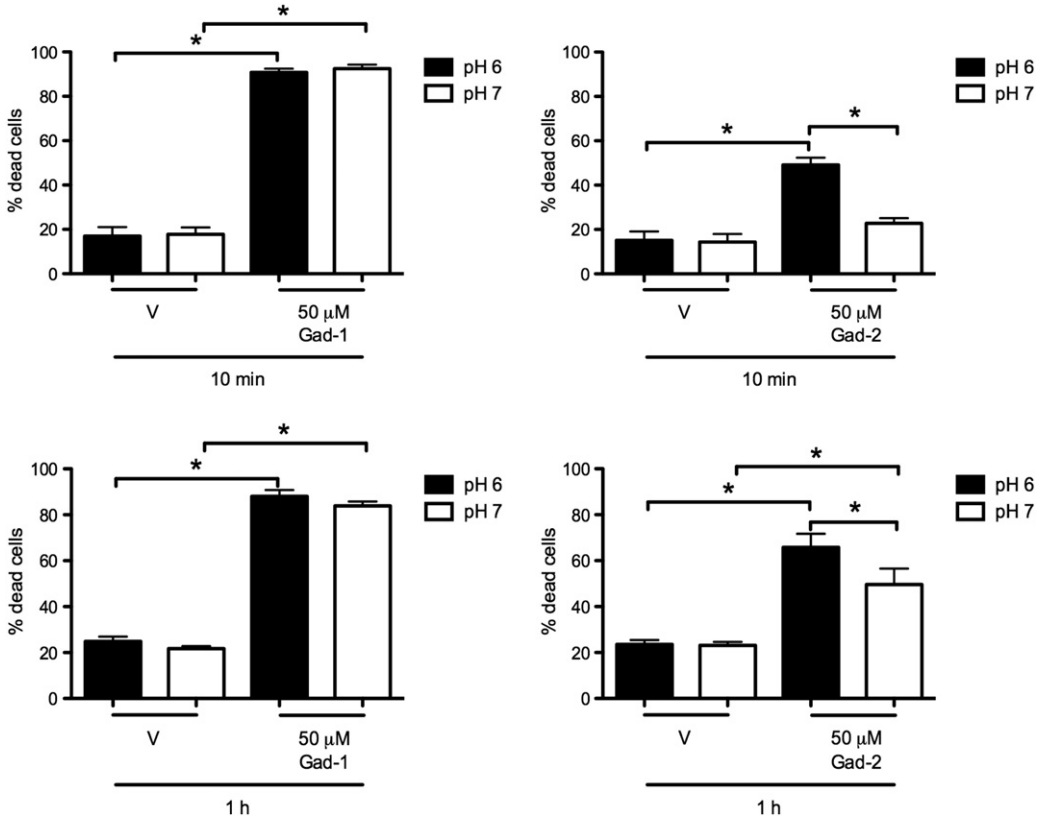

Fig. 3. Effect of Gad-1 and Gad-2 on U266 multiple myeloma cell viability. Cells were treated with vehicle control (V), 50 μM Gad-1 or Gad-2 in cRPMI at pH 6 or pH 7 for 10 min (upper panel) or 1 h (lower panel) and then stained with 7-AAD for 5 min before analysis by flow cytometry. Data shown are the mean of at least 3 independent experiments ± SEM; $^*p < 0.05$, determined by a one-way ANOVA with a Tukey–Kramer post-test.

well-structured proteins. Specifically, hydrogen bond restraints were not employed at all and helical dihedral angle restraints ($\varphi = -60 \pm 30°$ and $\psi = -40 \pm 40°$) were only employed for residues with a HA chemical shift index (CSI) < -0.25 ppm. The Gad-1 structure ensemble was calculated using 217 unambiguous NOEs and 48 ambiguous NOEs. The Gad-2 ensemble was calculated using 168 unambiguous NOEs and 77 ambiguous NOEs. Care was also taken to avoid overconstraining the structures by retaining too many low energy conformers. To this end only 20 structures of each peptide were calculated and the 7 lowest energy structures, which in both cases were the complete set of structure calculations with no restraint violations, were retained. The structures were calculated using Xplor NIH [38] with the input files sa.inp, anneal.inp and accept.inp.

3. Results

3.1. Functional studies with Gad-1 and Gad-2

Minimal inhibitory concentrations (MICs) for the peptides against *E. coli* were measured at both pH 5 and pH 7 (Fig. 1). The activity of Gad-1 does not appear to be very pH dependent, as an MIC of 5.1 μM (12.5 μg/mL) was determined in 4 out of 6 repeated experiments at pH 5, and in 5 out of 6 experiments at pH 7. Gad-2 however, exhibited greater activity at pH 5 than at pH 7, with an MIC of 11.5 μM (25 μg/mL) in 4 out of 6 experiments at pH 5, but > 23.0 μM (50 μg/mL) in 4 out of 6 experiments at neutral pH. This is interesting considering that Gad-1 has five histidine residues and Gad-2 only four. At both pHs, Gad-1 was more active than Gad-2.

Hemolysis assays were performed to measure the activity of Gad-1 and Gad-2 against human RBCs (Fig. 2). The HC_{50}, i.e. the peptide concentration that causes 50% lysis of RBCs, was 43 μM for Gad-1 and 56 μM for Gad-2. Since there is a minimal amount of RBC lysis at the MIC values of the peptide, it appears that Gad-1 and Gad-2 are selective in their activity against bacteria.

Further studies were performed to examine Gad-1 and Gad-2 killing of multiple myeloma cells at acidic and neutral pH (Fig. 3). Similar to the *E. coli* MIC experiments, Gad-1 was more active than Gad-2 at both pHs, but Gad-2 was more sensitive to pH than Gad-1. A 50 μM concentration of Gad-1 killed 92% of the cells at pH 7 after 10 min incubation and there was no significant difference in cell killing at pH 6. Gad-2 killed 22% of

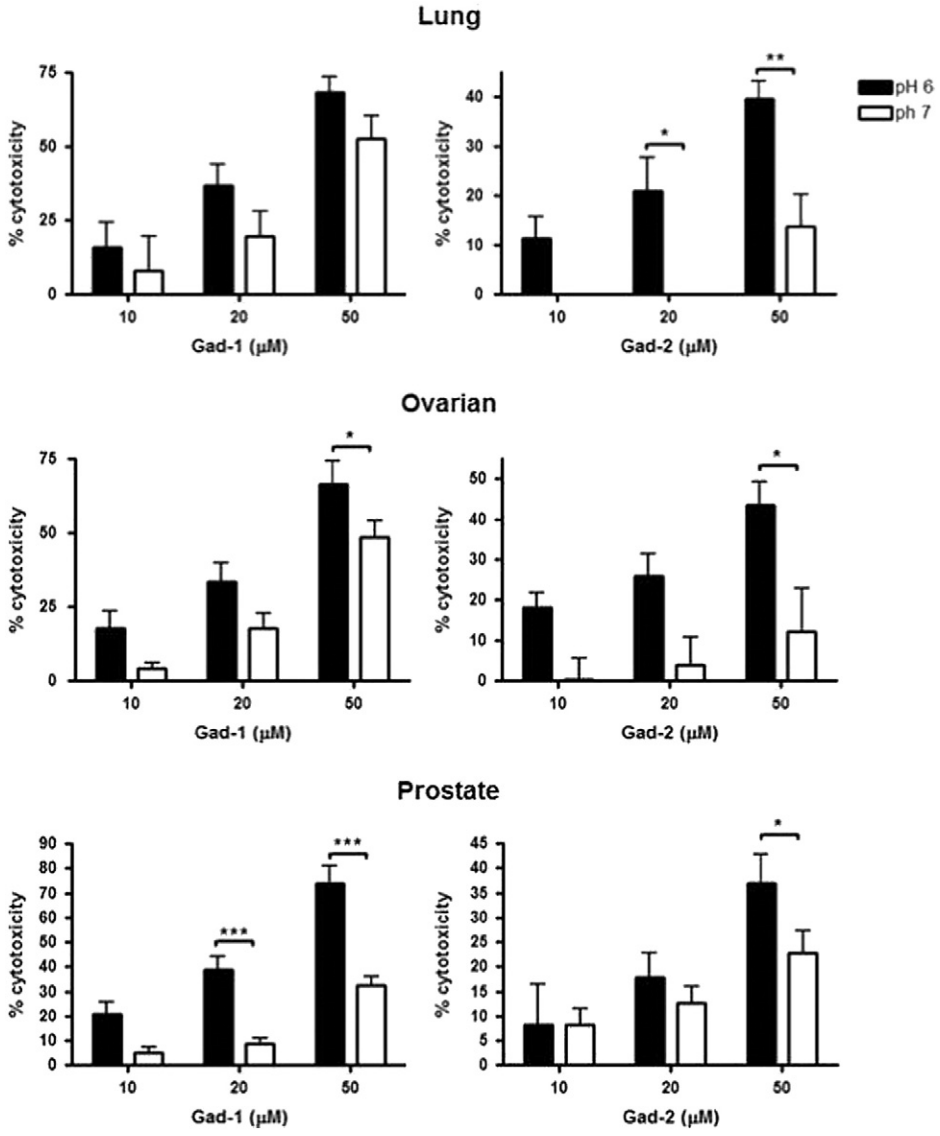

Fig. 4. Cytotoxic effect of Gad-1 and Gad-2 on carcinoma cells. Lung (LLC), ovarian (HEY), and prostate (PC3) carcinoma lines were treated with the indicated concentrations of Gad-1 or Gad-2 for 24 h at pH 6 or pH 7. Cell viability was then assessed by an MTT viability assay. Data are shown as the mean percent cytotoxicity (± SE), relative to vehicle-treated cells under their respective pH conditions, of at least 4 independent experiments. Statistical significance was determined by two-way ANOVA with a Bonferroni post-test. $^{*}p < 0.05$, $^{**}p < 0.01$, $^{***}p < 0.001$.

the cells at pH 7 and there was a statistically significant difference at pH 6, with 49% of the cells killed. Similar results were obtained with a one hour incubation time. Gad-1 is substantially more active in the multiple myeloma cell assays than it is in the human red blood cell assays; however, for Gad-2 the results are more comparable — at pH 7, Gad-2 appears to have similar activity against RBCs and multiple myeloma cells.

The anti-cancer properties of Gad-1 and Gad-2 against a range of carcinomas, under acidic and neutral pH conditions, were also investigated (Fig. 4). Both Gad-1 and Gad-2 demonstrated concentration-dependent cytotoxicity against LLC cells, HEY ovarian cancer cells, and PC3 prostate cancer cells. Consistent with the other functional studies, Gad-1 showed a greater cytotoxic effect compared to Gad-2. In contrast to the pH dependence of the results with *E. coli* and multiple myeloma cells, both peptides exhibited significantly greater killing of ovarian and prostate cells under acidic conditions (two-way ANOVA, $p < 0.05$), while Gad-2 showed a significant pH-dependent alteration in activity with all three carcinoma cell lines. The pH-dependent effect was more pronounced with Gad-2 than Gad-1 in LLC and ovarian cancer cells in which peptide-mediated killing at 50 μM was increased by approximately four-fold under acidic conditions.

3.2. Secondary structure dependence on environment

Circular dichroism experiments were performed with Gad-1 and Gad-2 in order to elucidate their conformational preferences in a variety of environments and pHs (Fig. 5). Percent helicity was also estimated from the ellipticity value at 222 nm [35] (Table 1). In zwitterionic LUVs composed of POPC, the degree of helicity is similar at pH 5, 6, and 7 and is on average 38% for Gad-1 and 11% for Gad-2. On the other hand, in anionic POPG LUVs, the helicity is strongly dependent on pH with % helicity for Gad-1 running from 56% at pH 5 to 100% at pH 7 and for Gad-2 running from 19% at pH 5 to 100% at pH 7. As LUVs are not suitable for high resolution, solution NMR structural work, comparisons were also made to solution NMR compatible solvents including 20% TFE and SDS micelles at pH 5. SDS micelles were chosen for high resolution structure determination of the Gad peptides as this environment induces an intermediate level of peptide structuring.

3.3. NMR structure determination

Solution NMR data was collected for Gad-1 and Gad-2 in 150 mM SDS micelles at pH 5. Chemical shift assignments employed 2D-NOESY and 2D-TOCSY data acquired at 35 °C, with help from data at 40 and 45 °C to resolve overlap. All of the expected resonances could be assigned, with the exception of Gad-1 Phe1. Notably, HD2 (C2) resonances were observed for all histidine residues in Gad-1 and Gad-2, confirming that all the histidines are indeed in their protonated form under these conditions [39].

Secondary structure indicators, including chemical shift index (CSI) and NOE patterns are summarized in Fig. 6. More negative CSI values for Gad-1 compared to Gad-2 indicate a greater helical propensity for Gad-1. A greater overall helicity for Gad-1 is also supported by greater numbers of NOEs between residues spaced 3 and 4 residues apart, as well as the higher number of strong sequential HN–HN NOEs observed for Gad-1 compared to Gad-2 — which are indicative of helical structure [37].

Structure calculations were carried out based on 265 inter-residue NOEs for Gad-1 and 245 inter-residues NOEs for Gad-2. Particular care was taken to calculate structure ensembles with the largest variety of structures consistent with the experimental data — to avoid over-constraining the structures. While typical NMR structure calculations normally employ both dihedral and hydrogen bond restraints, for Gad-1 and Gad-2 we did not employ any hydrogen bond restraints and added helical dihedral angle restraints only for residues with CSI < −0.25 ppm (Fig. 6).

The resulting structure ensemble for Gad-1 is well ordered over the C-terminal 17 residues (backbone RMSD for residues 5–21 = 0.39 Å) and more structurally heterogeneous for the N-terminal 4 residues

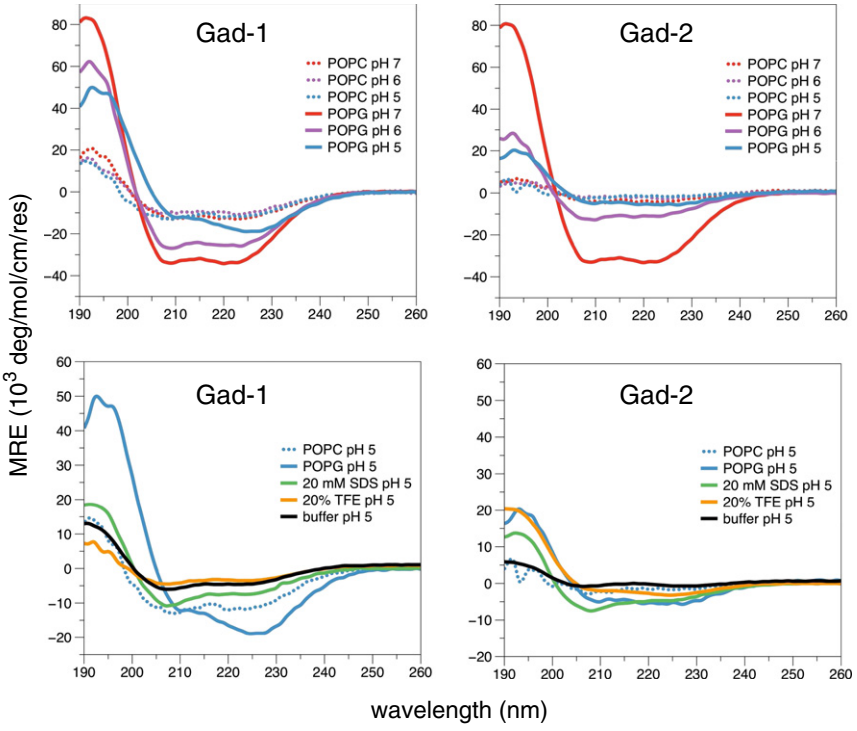

Fig. 5. Far-UV CD spectra of Gad-1 and Gad-2 at 25 °C.

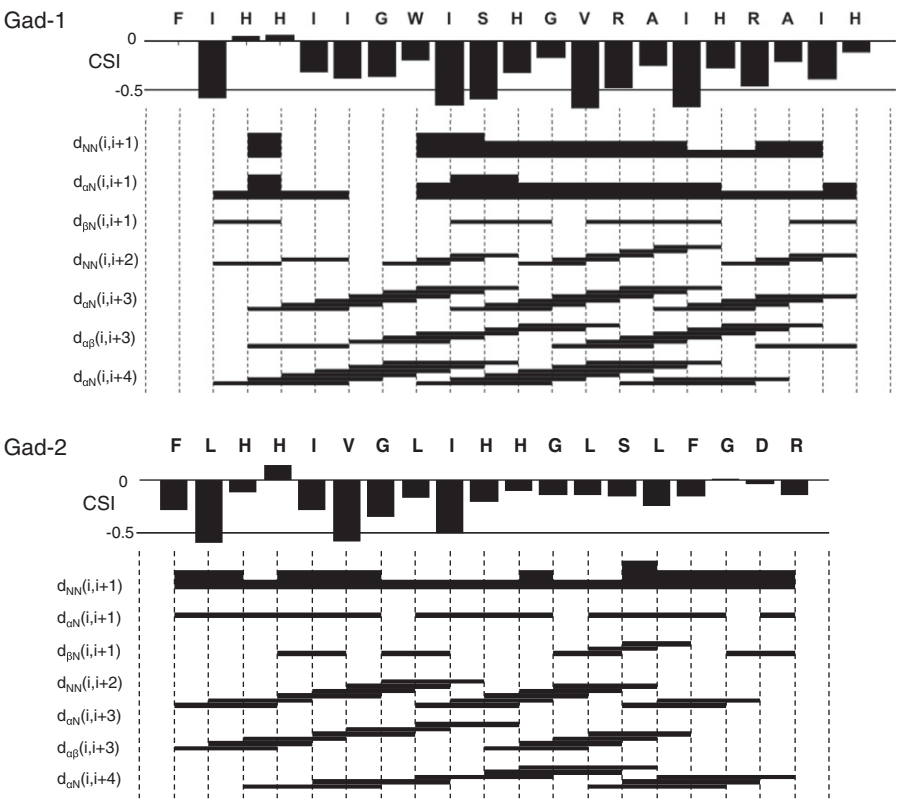

Fig. 6. Secondary structure indicators for Gad-1 and Gad-2 in SDS micelles at 35 °C. The upper panels display chemical shift index (CSI). Lower panels indicate NOEs. The interaction strengths for the $HN_i - HN_{i+1}$ and $HA_i - HN_{i+1}$ NOEs are indicated by the height of the bars as strong, medium or weak. All other interactions are indicated by their presence or absence.

(Fig. 7A). Gad-1 takes on a helical secondary structure from residues 6 to 9 and residues 12 to 20 (Fig. 7B). For the most homogeneously structured part of the peptide, i.e. residues 5 to 21, there is well-defined partitioning of hydrophobic sidechains to one side of the peptide and hydrophilic sidechains to the opposite face (Fig. 7C). The tryptophan residue, which is itself amphipathic and potentially quite important for function [40], locates to the interface between the polar and non-polar faces of the peptide. The break in the helix occurs at Serine 10/Histidine 11.

As expected from the circular dichroism data, the ensemble of calculated structures for Gad-2 is much more disordered than for Gad-1, with a backbone RMSD of 1.5 Å for residues 5 to 19 (Fig. 8). Like Gad-1, Gad-2 is also most structurally heterogeneous in the N-terminal 4 residues. Even though all 7 lowest energy structures calculated for Gad-2 were consistent with the experimentally determined NMR data, the structures display a variety of secondary structures (with helical regions colored magenta in Fig. 8A). Residues 9–12 appear to have the strongest helical tendency — with helical structure in 5 out of 7 calculated structures. Residues 6–8 and 15–17 displayed weaker helical tendency with helical structure in 3 out of 7 and 2 out of 7 calculated structures, respectively. Thus, the central helical region tends to break at Glycine 13/Serine 14.

The Gad-1 and Gad-2 NMR data were examined for indications that the peptides might be forming dimers. However, no likely inter-peptide NOEs could be identified and comparison of 1D NMR spectra of samples with varying peptide concentration revealed no signs of oligomerization.

4. Discussion

By revealing structure-function relationships in Gad-1 and Gad-2, we are hoping to contribute knowledge about factors that influence the specificity of AMPs and thus to contribute to rational optimization of AMP sequences to improve their therapeutic ratios. Functional studies of Gad-1 and Gad-2 reveal that while Gad-1 has more activity than Gad-2 at all pH values tested, Gad-2's anti-*E. coli* activity is much more pH-dependent than Gad-1's (Fig. 1). Similarly, against the multiple myeloma and three carcinoma cell lines assayed, Gad-1 is always more active than Gad-2, regardless of pH. Interestingly, while Gad-2's activity was significantly pH-dependent in all four cancer cell lines, Gad-1 was also pH dependent in two of these, although the fold-change was not as much as for Gad-2 (Figs. 3 and 4). In exploring the mechanisms for Gad-2's strong pH sensitivity compared to Gad-1's mild pH sensitivity, we need to consider factors such as peptide structure, as well as both the hydrophobic and electrostatic components of peptide–lipid interactions.

Circular dichroism experiments allow us to compare the helicity of the peptides in a variety of lipid and other environments (Fig. 5). Lipid vesicles composed of POPC LUVs provide a crude mimic of non-cancerous eukaryotic cell membranes, which are composed largely of zwitterionic lipids. On the other hand, vesicles composed of the anionic lipid, POPG, reflect the character of the more negatively charged nature of the headgroups in many bacterial or cancer cell membranes [11], although only to a first approximation as bacterial membranes are typically composed largely of phosphatidylethanolamine and cardiolipin in addition to the PG, and also have a lipopolysaccharide (LPS) layer that is likely important for AMP interactions [41]. In zwitterionic POPC, there is little pH dependence of Gad-1 or Gad-2 helicity and the overall level of helical structuring is much lower than in POPG at any pH (Table 1). This indicates that the more robust electrostatic interactions between the peptides and the anionic PG headgroups compared to with the PC headgroups, have a strong influence on peptide structure.

Comparing the helicity of the peptides at pH 7, i.e., when the histidine sidechains are expected to be deprotonated, in POPG versus POPC reveals aspects of peptide–lipid interactions. Both peptides are 100% helical in POPG, but in POPC exhibit much less helicity; 42% for Gad-1 and 16% for Gad-2. This is in contrast to what we have observed before for

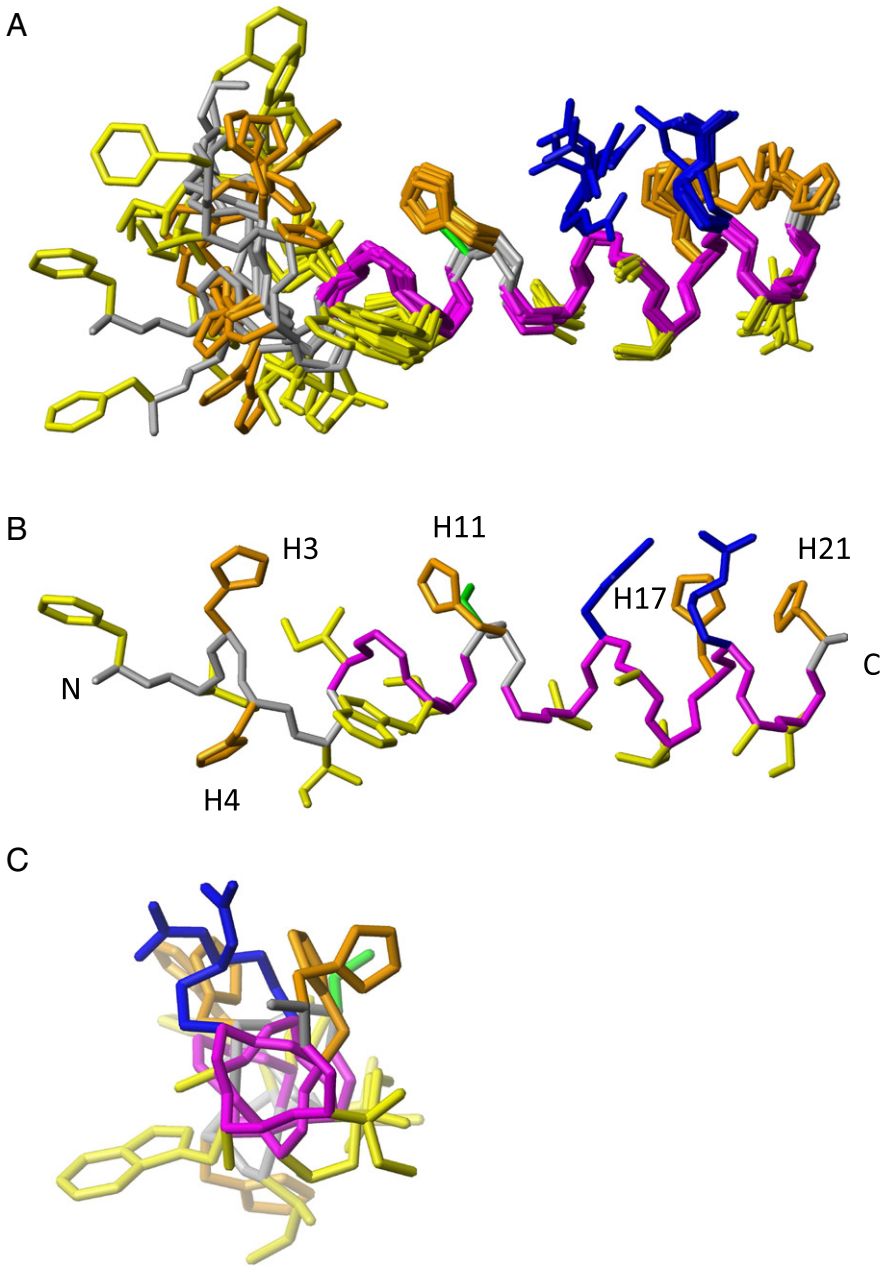

Fig. 7. 3D structure of Gad-1 with the helical portion of the backbone colored magenta, hydrophobic sidechains yellow, histidines orange, serine green and arginine blue. (A) Ensemble consisting of 7 individual structures that are consistent with the experimental data. (B) Representative structure with the histidines labeled. (C) Representative structure rotated by 90° to show the amphipathicity.

other antimicrobial peptides that exhibit the same structure in anionic and zwitterionic environments [42] and to the related peptide piscidin's observed behavior in structuring strongly helical in a zwitterionic environment [43]. On the other hand, similar to the Gads, LL37 has been observed to be random in POPC, but helical in a mix of POPC and POPG [44]. The major alteration in structure with lipid environment for the Gad peptides implies that charge interactions between PG and non-histidine-sidechain moieties on the peptide have a strong influence on peptide structure. The charged groups on Gad-1 at pH 7 would be the positively charged N-terminus and Arg-14 and Arg-18 sidechains. When completely helical, Gad-1 can form a perfectly helical structure with the N-terminus near the polar/apolar interface, and the arginines at the polar interface apparently forming helix-stabilizing interactions with the PG headgroups (Fig. 9). That much of the helical structure is lost in POPC indicates the importance to helix stabilization of the Arg/N-terminus interactions with PG.

With Gad-2 at pH 7, the charged moieties consist of the N-terminus, Arg-19, plus the negatively charged side chain of Asp-18, and thus both electrostatic attraction and repulsion come into play. The almost complete loss of helical structure upon switching from POPG into POPC indicates that interactions with the PG headgroups are key in inducing the helical structure. This behavior may relate to the disposition of the charged peptide groups. That is, the positively charged groups at the N-terminus and the Arg-19 sidechain locate to opposite ends of the polar/apolar interface of the peptide. However, the negatively charged Asp-18 locates near the center of the polar face where it would be repelled by the PG headgroups, but could have favorable interactions with PC headgroups (Fig. 9).

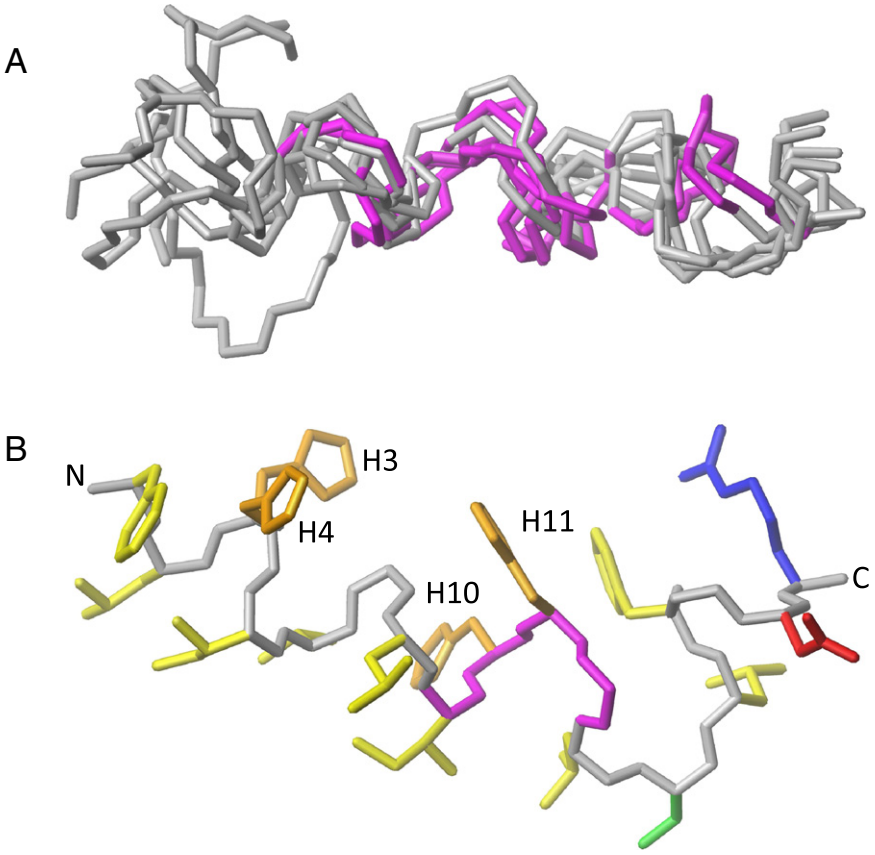

Fig. 8. 3D structure of Gad-2 with the helical portion of the backbone colored magenta, hydrophobic sidechains yellow, histidines orange, serine green, arginine blue and aspartate red. (A) Ensemble consisting of 7 individual structures that are consistent with the experimental data. Sidechains are omitted for clarity. (B) Representative structure with the histidines labeled.

Next, we turn to the experiments at acidic pH, which reveal the role of the positive charge on the histidines. In POPC, dropping the pH from 7 to 6 or 5 has very little effect on helicity. That is to say, the partial helical structuring observed in POPC (~38% for Gad-1 and ~11% for Gad-2) is largely unaffected by histidine charge — presumably because of the absence of strong electrostatic interactions with the PC headgroups. On the other hand, in anionic lipid, i.e. POPG LUVs, pH has a dramatic effect on the helicity of both peptides. While both peptides are 100% helical at pH 7, the helicity decreases dramatically as the pH is reduced — with Gad-1's helicity dropping to 56% at pH 5 and Gad-2's helicity dropping to 19% at pH 5. Gad-2's greater sensitivity of helicity to pH is in keeping with the greater sensitivity of its activity to pH.

It is notable that this decrease in Gad-2 helicity with reduced pH corresponds to an increase in activity. AMPs are frequently assumed to exhibit the opposite structure–function relationship — i.e. to become more active when they assume a helical structure, although this observation is far from universal. On the other hand, the general rule of "more helicity equals more activity" does seem to hold true when comparing Gad-1 to Gad-2 — Gad-1 is more functionally active than Gad-2 and also exhibits greater helicity in all the conditions tested. Therefore,

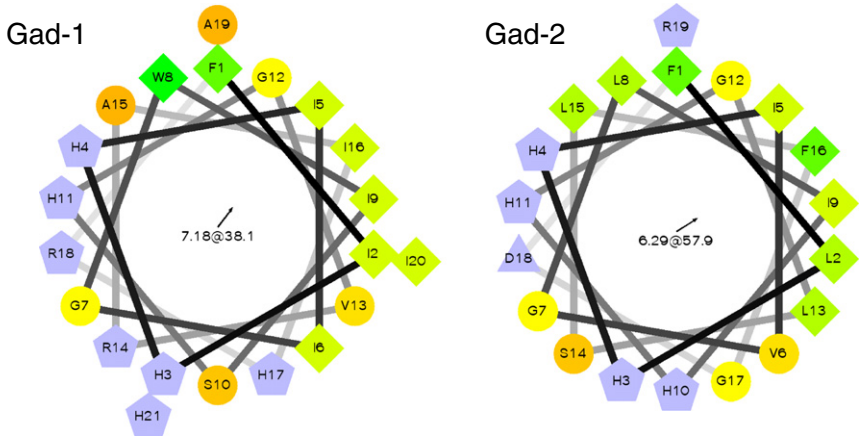

Fig. 9. Helical wheel plots [47] of Gad-1 and Gad-2 indicate well-defined amphipathicity when the peptides are 100% helical.

there appears to be no simple rule for correlating helicity with antimicrobial activity, at least for the Gad peptides.

Since the structure of Gad-1 and Gad-2 depend very much on the composition of their lipid environment, the high resolution structures determined (Figs. 7,8) are best viewed as "base" structures that indicate the structural tendencies under conditions where an intermediate level of helicity is present. In both peptides, the central and C-terminal regions show the strongest tendency to structure as an amphipathic helix, whereas the N-terminal regions are the most disordered and do not exhibit partitioning of the hydrophobic and polar residues. Such "imperfect amphipathicity" has been suggested to be important to disruption of membranes by AMPs [45]. For Gad-2, which demonstrates extreme sensitivity of its structure and activity with histidine charge, it may be that the "imperfect amphipathicity" induced by lowering the pH and hence disrupting the anionic-lipid bound structure, is critical to achieving the right balance of amphipathicity with imperfection in order to maximize the activity. As to why Gad-2 is more sensitive to pH than Gad-1 even though Gad-1 has five histidine residues to Gad-2's four, we suggest the answer lies with the overall charge balance of the two peptides, which is quite different at neutral pH. Gad-1 carries a charge of +3 at pH 7 and +8 at pH 5, whereas Gad-2 has a charge of only +1 at neutral pH and +5 at pH 5. Consistent with this suggestion, Kharidia et al. have observed pH-dependent MICs only in the least positively charged members of two different histidine-containing peptide families [22]. In addition to the role of histidine's positive charge in altering the lipid-peptide interactions of the Gads discussed above, our earlier simulation studies indicated a special role for sequential pairs of histidines [46]. In the simulations, sequential pairs of histidines, but not single histidines, display a strong preference to closely associate with bilayer pores, and this preference persists even if the histidines are uncharged. Thus Gad-2, with its two pairs of histidines, compared to Gad-1, with only one histidine pair, may be poised close to a threshold for membrane disruption; only a small change in electrostatic interactions (e.g. histidine protonation and/or increase in anionic lipid constituents) is required to activate antimicrobial activity.

In summary, our work demonstrates a higher level of pH dependence of bacterial growth inhibition and cancer cell killing for the AMP Gad-2 in comparison to Gad-1, both histidine-rich peptides. When considering the mechanism for this functional tuning, it is important to keep in mind that while lipid-AMP interactions are central in AMP function, model membrane studies such as this one do not address potentially important interactions with other cell envelope components including lipopolysaccharide and peptidoglycan. None-the-less, the greater functional plasticity observed for Gad-2 correlates with a greater structural plasticity. While both Gad-1 and Gad-2 demonstrated different levels of helicity depending on pH and lipid environment, Gad-2 shows much more drastic structural changes. Interestingly, the pH with the highest level of Gad-2 functional activity does not correspond to the pH with the greatest helicity, indicating that the most functional conformation of Gad-2 is not necessarily the most helical, perfectly amphipathic structure. We propose instead that a balance between amphipathic and mixed hydrophobic/hydrophilic structural features are needed for maximal activity. Other factors that may influence Gad-2's more finely tuned structure-functional relationships include that its histidines appear in pairs, rather than singly, as well as Gad-2's lower overall positive charge at pH 7. Thus, this examination of the Gad peptides, along with our earlier simulation study [46], suggest that in trying to improve the therapeutic ratio of other AMPs in development, consideration should be given to including histidine-pairs, keeping the overall charge of the peptide modest, and retaining a degree of structural plasticity and imperfect amphipathicity.

Transparency document

The Transparency document associated with this article can be found in the online version.

Acknowledgements

We are grateful to Dr. Celine Schneider for technical NMR expertise and to Dr. Rob Brown for help with the activity assays. Funding for this study was provided by Natural Sciences and Engineering Research Council of Canada (NSERC) Discovery Grants, as well as Canada Research Chairs, to VB and MLR, and a grant to DH from the Dalhousie Medical Research Foundation. LM is supported by a Postdoctoral Fellowship from the Canadian Breast Cancer Foundation-Atlantic Region.

References

[1] J. Wiesner, A. Vilcinskas, Antimicrobial peptides: the ancient arm of the human immune system, Virulence 1 (2010) 440–464.
[2] P. Bulet, R. Stocklin, L. Menin, Anti-microbial peptides: from invertebrates to vertebrates, Immunol. Rev. 198 (2004) 169–184.
[3] K. De Smet, R. Contreras, Human antimicrobial peptides: defensins, cathelicidins and histatins, Biotechnol. Lett. 27 (2005) 1337–1347.
[4] W.C. Wimley, K. Hristova, Antimicrobial peptides: successes, challenges and unanswered questions, J. Membr. Biol. 239 (2011) 27–34.
[5] H.W. Boucher, G.H. Talbot, J.S. Bradley, J.E. Edwards, D. Gilbert, L.B. Rice, M. Scheld, B. Spellberg, J. Bartlett, Bad bugs, no drugs: no ESKAPE! An update from the Infectious Diseases Society of America, Clin. Infect. Dis. 48 (2009) 1–12.
[6] P.C. Oyston, M.A. Fox, S.J. Richards, G.C. Clark, Novel peptide therapeutics for treatment of infections, J. Med. Microbiol. 58 (2009) 977–987.
[7] K. Matsuzaki, Control of cell selectivity of antimicrobial peptides, Biochim. Biophys. Acta 1788 (2009) 1687–1692.
[8] M.J. Browne, C.Y. Feng, V. Booth, M.L. Rise, Characterization and expression studies of Gaduscidin-1 and Gaduscidin-2; paralogous antimicrobial peptide-like transcripts from Atlantic cod (*Gadus morhua*), Dev. Comp. Immunol. 35 (2011) 399–408.
[9] K. Chikakane, H. Takahashi, Measurement of skin pH and its significance in cutaneous diseases, Clin. Dermatol. 13 (1995) 299–306.
[10] S. Al-Benna, Y. Shai, F. Jacobsen, L. Steinstraesser, Oncolytic activities of host defense peptides, Int. J. Mol. Sci. 12 (2011) 8027–8051.
[11] D.W. Hoskin, A. Ramamoorthy, Studies on anticancer activities of antimicrobial peptides, Biochim. Biophys. Acta 1778 (2008) 357–375.
[12] T. Xu, S.M. Levitz, R.D. Diamond, F.G. Oppenheim, Anticandidal activity of major human salivary histatins, Infect. Immun. 59 (1991) 2549–2554.
[13] R.J. Baumann, G.D. Mayer, L.D. Fite, L.M. Gill, B.L. Harrison, In vitro and in vivo candicidal activities of 2-(p-n-hexylphenylamino)-1,3-thiazoline, Chemotherapy 37 (1991) 157–165.
[14] C.J. Park, C.B. Park, S.S. Hong, H.S. Lee, S.Y. Lee, S.C. Kim, Characterization and cDNA cloning of two glycine- and histidine-rich antimicrobial peptides from the roots of shepherd's purse, *Capsella bursa-pastoris*, Plant Mol. Biol. 44 (2000) 187–197.
[15] I.K. Poon, K.K. Patel, D.S. Davis, C.R. Parish, M.D. Hulett, Histidine-rich glycoprotein: the Swiss Army knife of mammalian plasma, Blood 117 (2011) 2093–2101.
[16] F.D. Silva, C.A. Rezende, D.C. Rossi, E. Esteves, F.H. Dyszy, S. Schreier, F. Gueiros-Filho, C.B. Campos, J.R. Pires, S. Daffre, Structure and mode of action of microplusin, a copper II-chelating antimicrobial peptide from the cattle tick *Rhipicephalus* (*Boophilus*) *microplus*, J. Biol. Chem. 284 (2009) 34735–34746.
[17] R. Lai, H. Takeuchi, L.O. Lomas, J. Jonczy, D.J. Rigden, H.H. Rees, P.C. Turner, A new type of antimicrobial protein with multiple histidines from the hard tick, *Amblyomma hebraeum*, FASEB J. 18 (2004) 1447–1449.
[18] I.H. Lee, Y. Cho, R.I. Lehrer, Effects of pH and salinity on the antimicrobial properties of clavanins, Infect. Immun. 65 (1997) 2898–2903.
[19] E.J. van Kan, R.A. Demel, E. Breukink, A. van der Bent, B. de Kruijff, Clavanin permeabilizes target membranes via two distinctly different pH-dependent mechanisms, Biochemistry 41 (2002) 7529–7539.
[20] Z. Tu, A. Young, C. Murphy, J.F. Liang, The pH sensitivity of histidine containing lytic peptides, J. Pept. Sci. 15 (2009) 790–795.
[21] L. Kacprzyk, V. Rydengard, M. Morgelin, M. Davoudi, M. Pasupuleti, M. Malmsten, A. Schmidtchen, Antimicrobial activity of histidine-rich peptides is dependent on acidic conditions, Biochim. Biophys. Acta 1768 (2007) 2667–2680.
[22] R. Kharidia, Z. Tu, L. Chen, J.F. Liang, Activity and selectivity of histidine-containing lytic peptides to antibiotic-resistant bacteria, Arch. Microbiol. 194 (2012) 769–778.
[23] J. Georgescu, V.H. Munhoz, B. Bechinger, NMR structures of the histidine-rich peptide LAH4 in micellar environments: membrane insertion, pH-dependent mode of antimicrobial action, and DNA transfection, Biophys. J. 99 (2010) 2507–2515.
[24] J. Ruangsri, S.A. Salger, C.M. Caipang, V. Kiron, J.M. Fernandes, Differential expression and biological activity of two piscidin paralogues and a novel splice variant in Atlantic cod (*Gadus morhua* L.), Fish Shellfish Immunol. 32 (2012) 396–406.
[25] B.J. Sun, H.X. Xie, Y. Song, P. Nie, Gene structure of an antimicrobial peptide from mandarin fish, *Siniperca chuatsi* (Basilewsky), suggests that moronecidins and pleurocidins belong in one family: the piscidins, J. Fish Dis. 30 (2007) 335–343.
[26] E.Y. Chekmenev, B.S. Vollmar, K.T. Forseth, M.N. Manion, S.M. Jones, T.J. Wagner, R.M. Endicott, B.P. Kyriss, L.M. Homem, M. Pate, J. He, J. Raines, P.L. Gor'kov, W.W. Brey, D.J. Mitchell, A.J. Auman, M.J. Ellard-Ivey, J. Blazyk, M. Cotten, Investigating molecular recognition and biological function at interfaces using piscidins, antimicrobial peptides from fish, Biochim. Biophys. Acta 1758 (2006) 1359–1372.
[27] A.A. De Angelis, C.V. Grant, M.K. Baxter, J.A. McGavin, S.J. Opella, M.L. Cotten, Amphipathic antimicrobial piscidin in magnetically aligned lipid bilayers, Biophys. J. 101 (2011) 1086–1094.

[28] S.A. Lee, Y.K. Kim, S.S. Lim, W.L. Zhu, H. Ko, S.Y. Shin, K.S. Hahm, Y. Kim, Solution structure and cell selectivity of piscidin 1 and its analogues, Biochemistry 46 (2007) 3653–3663.
[29] G. Idiong, A. Won, A. Ruscito, B.O. Leung, A.P. Hitchcock, A. Ianoul, Investigating the effect of a single glycine to alanine substitution on interactions of antimicrobial peptide latarcin 2a with a lipid membrane, Eur. Biophys. J. 40 (2011) 1087–1100.
[30] L.S. Vermeer, Y. Lan, V. Abbate, E. Ruh, T.T. Bui, L.J. Wilkinson, T. Kanno, E. Jumagulova, J. Kozlowska, J. Patel, C.A. McIntyre, W.C. Yam, G. Siu, R.A. Atkinson, J.K. Lam, S.S. Bansal, A.F. Drake, G.H. Mitchell, A.J. Mason, Conformational flexibility determines selectivity and antibacterial, antiplasmodial, and anticancer potency of cationic alpha-helical peptides, J. Biol. Chem. 287 (2012) 34120–34133.
[31] B. Bechinger, C. Aisenbrey, The polymorphic nature of membrane-active peptides from biophysical and structural investigations, Curr. Protein Pept. Sci. 13 (2012) 602–610.
[32] L.T. Nguyen, E.F. Haney, H.J. Vogel, The expanding scope of antimicrobial peptide structures and their modes of action, Trends Biotechnol. 29 (2011) 464–472.
[33] K.A. Brogden, Antimicrobial peptides: pore formers or metabolic inhibitors in bacteria? Nat. Rev. Microbiol. 3 (2005) 238–250.
[34] J.T. Yang, C.S. Wu, H.M. Martinez, Calculation of protein conformation from circular dichroism, Methods Enzymol. 130 (1986) 208–269.
[35] C.A. Rohl, R.L. Baldwin, Comparison of NH exchange and circular dichroism as techniques for measuring the parameters of the helix-coil transition in peptides, Biochemistry 36 (1997) 8435–8442.
[36] Goddard, T. D., Kneller, D. G., Sparky 3, University of California, San Francisco. https://www.cgl.ucsf.edu/home/sparky/.
[37] K. Wuthrich, NMR of Proteins and Nucleic Acids, Wiley-Interscience, New York, 1986.
[38] C.D. Schwieters, J.J. Kuszewski, N. Tjandra, G.M. Clore, The Xplor-NIH NMR molecular structure determination package, J. Magn. Reson. 160 (2003) 65–73.
[39] B.F. Edwards, B.D. Sykes, Assignment and characterization of the histidine resonances in the 1H nuclear magnetic resonance spectra of rabbit tropomyosins, Biochemistry 17 (1978) 684–689.
[40] O. Rekdal, B.E. Haug, M. Kalaaji, H.N. Hunter, I. Lindin, I. Israelsson, T. Solstad, N. Yang, M. Brandl, D. Mantzilas, H.J. Vogel, Relative spatial positions of tryptophan and cationic residues in helical membrane-active peptides determine their cytotoxicity, J. Biol. Chem. 287 (2012) 233–244.
[41] R.M. Epand, R.F. Epand, Bacterial membrane lipids in the action of antimicrobial agents, J. Pept. Sci. 17 (2011) 298–305.
[42] S. Bourbigot, E. Dodd, C. Horwood, N. Cumby, L. Fardy, W.H. Welch, Z. Ramjan, S. Sharma, A.J. Waring, M.R. Yeaman, V. Booth, Antimicrobial peptide RP-1 structure and interactions with anionic versus zwitterionic micelles, Biopolymers 91 (2009) 1–13.
[43] S. Campagna, N. Saint, G. Molle, A. Aumelas, Structure and mechanism of action of the antimicrobial peptide piscidin, Biochemistry 46 (2007) 1771–1778.
[44] S. Thennarasu, A. Tan, R. Penumatchu, C.E. Shelburne, D.L. Heyl, A. Ramamoorthy, Antimicrobial and membrane disrupting activities of a peptide derived from the human cathelicidin antimicrobial peptide LL37, Biophys. J. 98 (2010) 248–257.
[45] M. Mihajlovic, T. Lazaridis, Antimicrobial peptides bind more strongly to membrane pores, Biochim. Biophys. Acta 1798 (2010) 1494–1502.
[46] M.H. Khatami, M. Bromberek, I. Saika-Voivod, V. Booth, Molecular dynamics simulations of histidine-containing cod antimicrobial peptide paralogs in self-assembled bilayers, Biochim. Biophys. Acta 1838 (2014) 2778–2787.
[47] http://rzlab.ucr.edu/scripts/wheel.